IEEE Access
Multidisciplinary | Rapid Review | Open Access Journal

Received 12 September 2023, accepted 12 October 2023, date of publication 18 October 2023, date of current version 27 October 2023.

Digital Object Identifier 10.1109/ACCESS.2023.3325478

RESEARCH ARTICLE

Performance Prediction in UAV-Terrestrial Networks With Hardware Noise

BUI VU MINH[1], ANH-TU LE[2], (Member, IEEE), CHI-BAO LE[3], SANG QUANG NGUYEN[4], VAN-DUC PHAN[5], TAN N. NGUYEN[6], (Member, IEEE), AND MIROSLAV VOZNAK[2], (Senior Member, IEEE)

[1]Faculty of Engineering and Technology, Nguyen Tat Thanh University, Ho Chi Minh City 754000, Vietnam
[2]Faculty of Electrical Engineering and Computer Science, VSB—Technical University of Ostrava, 70800 Ostrava, Czech Republic
[3]Transcosmos Vietnam, Ho Chi Minh City 700000, Vietnam
[4]Science and Technology Application for Sustainable Development Research Group, Ho Chi Minh City University of Transport, Ho Chi Minh City 70000, Vietnam
[5]Faculty of Automotive Engineering, School of Technology, Van Lang University, Ho Chi Minh City 70000, Vietnam
[6]Communication and Signal Processing Research Group, Faculty of Electrical and Electronics Engineering, Ton Duc Thang University, Ho Chi Minh City 70000, Vietnam

Corresponding author: Van-Duc Phan (duc.pv@vlu.edu.vn)

This research was financially supported by Van Lang University, Vietnam. The research was also co-funded by the European Union within the REFRESH project - Research Excellence For Region Sustainability and High-tech Industries ID No. CZ.10.03.01/00/22_003/0000048 of the European Just Transition Fund and by the Ministry of Education, Youth and Sports of the Czech Republic (MEYS CZ) through the e-INFRA CZ project (ID:90254) and also by the MEYS CZ within the project SGS ID No. SP 7/2023 conducted by VSB-Technical University of Ostrava.

ABSTRACT To enhance the service quality of the unmanned aerial vehicle (UAV), the UAV-aided Internet of Things (IoT) systems could deploy a Deep Neural Network (DNN) for performance prediction for the users. Non-orthogonal multiple access (NOMA) is applied to such networks in order to improve spectrum efficiency, and results in improved quality of service at the ground users under the mobility of UAV. The outage and ergodic capacity requirements of the IoT users may not be satisfied due to some imperfect system parameters such as hardware noise. A DNN-based algorithm for performance prediction and the design of multiple antennas at the UAV under hardware noise is proposed. In this DNN-based UAV-NOMA, the central controller (server) collects system parameters periodically based on observing the state of IoT system and performs adjustments to the dynamic environment. The closed-form expressions for the outage probability and the ergodic capacity are derived to evaluate the performance of a group of IoT users. Our numerical results demonstrate that: i) In contrast to the traditional UAV-NOMA system, the UAV cannot know the performance at each IoT user in order to adjust the parameters (i.e. power allocation factors) before transmitting the signals to the devices; while the proposed DNN-based IoT system is capable of predicting the performance; ii) The performance of the IoT users can be significantly improved by integrating more antennas at the UAV and limiting levels of hardware noise; iii) By designing NOMA, the UAV-NOMA-based IoT system can increase the throughput to the tune of 40% compared with the benchmark (the orthogonal multiple access (OMA)-based IoT).

INDEX TERMS Deep neural networks, non-orthogonal multiple access (NOMA), line-of-sight (LoS), unmanned aerial vehicles (UAVs), the Internet of Things (IoT), hardware noise.

I. INTRODUCTION

Viewed as important components in the development of the beyond-fifth-generation (B5G)/sixth-generation (6G) communications infrastructure, satellites/constellations and aerial platforms, and their interactions with terrestrial networks have attracted significant interest in recent years in part due to their capability of accommodating flexible deployment and ubiquitous access [1], [2]. To satisfy stringent service requirements in traditional cellular systems, the cellular-based

The associate editor coordinating the review of this manuscript and approving it for publication was Alicia Fornés.

unmanned aerial vehicles (UAVs) can be considered as a new kind of user equipment and bring significant revenues for the operators [3]. Developing UAVs is also a new way to manage disaster zones where traditional cellular systems cannot work effectively [4]. In these applications, UAVs can provide services to the ground users by deploying the Low-Altitude Platform (LAP) or the High-Altitude Platform (HAP) [5]. On the other hand, UAVs are able to communicate with the associated terrestrial base stations (BSs) to assist cellular networks in applications such as aerial surveillance, cargo delivery, monitoring, and remote sensing. As another benefit, the ground users can maintain a stable connection with the UAV experiencing the Line-of-Sight (LoS) link. To implement these stable connections, the UAV can act as a mobile relay [6], [7], or a flying base station [8], [9]. In particular, the work in [8] deployed a dense network enabled by flying UAV-assisted base stations (BSs) to better serve ground users, and found the optimal location of the UAVs to maximize experiences of the users with expected data rates under the assumption of ordered users. The model in [9] deploys a UAV to fly cyclically along the distant users and play the role of a flying BS to offload data for users. UAV-assisted systems can be extended to integrate existing systems such as mmwave communication, reconfigurable intelligent surfaces, and Free-Space Optical (FSO) communication. The authors in [10] developed UAV-assisted free-space optical (FSO) communication systems to evaluate the system performance of UAV communications. They presented closed-form formulas of key system performance metrics such as the outage probability, the ergodic capacity, and the average bit error rate (BER) with various modulation schemes. Although UAVs exhibit their advantages as flying BSs, we still need to know how a UAV effectively allocates its transmit power to signals transferring to the ground users in order to improve spectrum and energy efficiency. Further, one of the challenging issues in UAV-aided communication networks is how to deploy UAVs to better provide reasonable coverage to ground users.

To improve spectrum efficiency in UAV-assisted communications, non-orthogonal multiple access (NOMA) is viewed as a promising solution to assist multi-UAV communications networks. Mirbolouk et al studied a hybrid satellite-UAV relay network. In this scenario, the UAV relays (URs) implement coordinated multi-point transmission to communicate with the ground users [11]. The authors in [12] presented (UAV)-assisted terrestrial-satellite communication systems by employing a multiantenna multiuser UAV over mixed free space optics (FSO)/radiofrequency (RF) channels. The RF links related to UAV connections follow the Nakagami-m distribution and their received signals are analyzed in terms of outage probability, asymptotic outage probability, ergodic capacity, effective capacity, and generalized average symbol-error-rate with various quadrature amplitude modulation (QAM) schemes.

Wang et al. [13] introduced a device-to-device architecture in NOMA-UAV networks to improve the data transfer efficiency by studying an algorithm of resource allocation relying on graph theory. Li et al. [14] investigated the performance of multiple users in a large NOMA network when UAV relaying plays an important role to amplify the forwarded interaction information to the ground users. Zhao et al. [15] presented the optimal sum-rate obtained by optimizing both resource allocation and the UAV trajectory. Budhiraja et al. [16] explored the mobile edge computing network relying on UAVs to minimize the energy consumption in terms of computational power, time and trajectory. In these aforementioned works, the design of a single-antenna UAV-mounted BS has limited performance, while we can leverage the evolution of multiple-antenna technology to empower operations of the UAV. Therefore, it is importance to study how the multiple-antenna UAV-mounted BS enhance the system performance by considering the benefits provided by multiple-antennas networks. Thus, researchers paid attention to explore the performance of multiple-antenna fitted UAV-mounted BS aided communication. For example, a multi-input single-output (MISO) UAV-BS system was developed in [17] and a robust power allocation approach was introduced to minimize power consumption and optimize trajectory and transmit beamforming vector. Further, the authors in [18] optimized the UAV trajectory in multi-antenna UAV-aided systems where cognitive radio is empowered to improve spectrum efficiency. The authors in [19] studied a UAV-assisted multiuser communication system to enable a multi-antenna UAV as a BS to serve multiple single-antenna ground users. Further, both orthogonal multiple access (OMA) and NOMA signals can be coordinated to develop a clustering-based hybrid multiple access technique to transmit the information to all ground users simultaneously.

The strong assumption of the perfect transmitter-receiver hardware architecture is a common theme across the aforementioned research efforts, however, it is utopian for real-practical applications. In practice, I/Q imbalance (IQI), high power amplifier (HPA) non-linearities, and oscillator phase noises may affect the hardware of wireless transceivers [20]. In addition, the transmit/receive signal is always accompanied by a little degree of unaccounted-for distortion brought on by residual hardware noise (RHN) [21]. In [22], NOMA-assisted satellite communication with UAV relaying is investigated. In addition, the author considered a real-life scenario as imperfect hardware issues in UAV relaying and ground users. Moreover, the closed-form OP is derived to evaluate the system performance of NOMA users. In [23], the authors expressed the exact and asymptotic formulas of OP and the ergodic capacity of AF and DF relaying systems. Specifically, the RHN is developed for all nodes.

A. RELATED WORKS

The aforementioned studies on UAVs crucially assumed ideal hardware and unpredictable performance of the ground users. To make UAV-assisted IoT systems a reality, UAV-assisted BS with hardware noise is an active field of research.

An UAV-assisted NOMA multi-way relaying network was considered in [14] to evaluate the impact of the existence of the RHN at the transceivers. In particular, the authors derived the analytical expressions for the achievable sum-rate to exhibit the performance of the considered networks. In [24] considered security in UAV-assisted system when UAV plays a role as an aerial BS and transmits the signal to a protected zone containing the ground users in the existence of multiple ground eavesdroppers. Their numerical results confirmed that the hardware noise has a significant impact on the average secrecy rate. In contrast, eavesdroppers benefit from the imperfect hardware. In a similar work, Guo and An studied how hardware noise affects to the performance of the reconfigurable intelligent surface-assisted integrated satellite-UAV-terrestrial networks [25]. However, we need to answer how the system can predict the performance to help the UAV-mounted BS adjust its parameters to better serve the ground users; for example, the UAV can adjust the power allocation coefficients to satisfy performance requirements at each device. Although optimization approaches work, they would impose higher computational load on to the UAV.

To the best of our knowledge, a few studies have been focused on machine learning-based algorithms in UAV-assisted IoT networks [26], [27], [28]. The authors in [26] studied UAV-assisted IoT networks relying on mobile edge computation, in which a Markov decision process (MDP) scheme is deployed to characterize optimization problem of data and energy transfer for the UAV. In particular, the MDP model is solved to obtain the optimal strategies and further help the UAV collect data, deliver data, and to maximize the long-term utility of the UAV. In a similar work, Li et al leveraged partial observable MDP problem in [27] to model the UAVs' flight resource allocation. In this MDP, they described each state to demonstrate UAVs' adopted heights and battery levels. To make optimal decisions for each state and solve the online flight resource allocation problem, a deep reinforcement learning algorithm (Q-learning) was employed in [28]. In this case, the proposed scheme combined Q-learning with deep reinforcement learning is employed to considerably minimize the data loss. The authors in [29] developed a deep neural network (DNN) to accurately predict the outage performance of aerial reconfigurable intelligent surface-assisted wireless system.

B. MOTIVATIONS AND OUR CONTRIBUTIONS

Since the DNN models can precisely estimate the desired system performance metrics from high dimensional raw data, the UAV can leverage DNN for performance prediction in order to expedite real-time configurations in IoT networks even in dynamic environments and complex radio conditions. This paper is motivated by the above analysis and provides a framework to evaluate the system performance of UAV-NOMA IoT systems with hardware noise, followed by the deep learning evaluation of performance prediction.

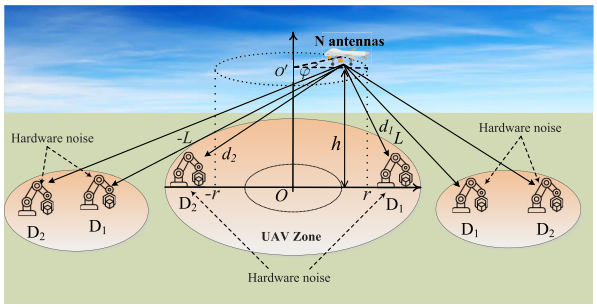

FIGURE 1. System Model.

Table 1 summarizes our article and the existing studies. Our contributions can be summarized as follows

- We design a multiple antennas UAV for applications in Iot system to enhance the energy efficiency compared with the normal system using multiple single-antenna UAVs.
- Such IoT system can leverage a DNN based UAV-NOMA framework for attaining the benefits of such performance predication since other unsupervised learning algorithms applied the normal operation of a IoT network do not leverage the data that can be achieved offline.
- We investigate performance at the ground users of both UAV-OMA case and UAV-NOMA case in the context of DNN based UAV system. Additionally, in contrast to the conventional UAV-NOMA, we deal with degraded performance under the impacts of hardware noise. Based on analysis of received signals, we derive the closed-form expressions for the outage probability, ergodic capacity and throughput of two IoT devices under the effect of LoS and NLoS probabilities. Then, we validate these derived expressions in various scenarios to find main parameters affecting to the system performance.

The rest of the paper is organized as follows. Section II presents the details of the proposed system model and assumptions. Section III analyzes the performance parameters including the outage probability, the throughput, and the ergodic capacity. Section IV introduces DNN method to predict the system performance. Section V presents the simulation results. Finally, section VI concludes the paper.

II. SYSTEM MODEL

A. HARDWARE NOISE MODEL

The broadcast and received signals are distorted by real-world RF transceivers that have IQ imbalances, amplifier non-linearities, and phase noise [37]. As a result, the signal model for these hardware flaws is modeled by

$$y = h(x + \eta_t + \eta_r) + n, \tag{1}$$

where x denotes the transmit signal, h denotes the channel model, and $\eta_t \sim \mathcal{CN}(0, P\kappa_t^2)$ and $\eta_r \sim \mathcal{CN}(0, P\kappa_r^2)$ denote the distortion noises at transmitter and receiver, respectively,

TABLE 1. Comparison between the novelty of our work and previous papers.

Ref./Prop.	Rician channel	Hardware noise	NOMA	Multiple Antennas UAV	Outage Probability	Ergodic Capacity	DNN
[32]	X	X	✓	X	✓	✓	X
[33]	X	X	✓	X	✓	X	X
[14]	X	✓	✓	X	X	✓	X
[34]	✓	X	X	X	✓	X	X
[19]	X	X	✓	✓	✓	X	X
[36]	✓	X	✓	X	✓	X	X
[37]	✓	X	✓	X	✓	X	X
[38]	X	X	✓	✓	✓	✓	X
Our study	✓	✓	✓	✓	✓	✓	✓

$P = \mathbb{E}[x^2]$, κ_t and κ_r are the design parameters attributed to the level of hardware noise.

B. DNN MODEL

In the DNN model, there are three layers which as the input layer, the multiple hidden layers and the output layer. The function of each layer in the DNN model training may be summed up as follows:

1) The Input Layer: Data is provided to the input layer so that the DNN model can determine how system parameters and performance are related. As a result, the number of neurons in the input layer is equal to the number of network parameters and does not serve as an activation function.
2) The Hidden Layer: The relationship between input data and output data is primarily calculated by many hidden layers. Therefore, for the relation to be calculated correctly, each connection in each hidden neuron has a separate weight and bias. Each hidden neuron also includes a nonlinear activation function to enhance computational performance.
3) The Output Layer:By combining the findings of several hidden layers, the output layer forecasts the system performance. As a result, the output layer is made up of just one neuron. The output layer's neuron is similar to the input layer's in that it lacks an activation function.

C. SIGNAL COMMUNICATION MODEL

We study the popular IoT application of aerial BS when a multiple-antenna UAV (denoted as R) is deployed to provide improved performance for a group of M ground IoT users, shown in Figure 1. We consider the scenario in which the UAV follows a circular trajectory and hovers to communicate with the IoT users in a sequential manner. In the context of IoT, the system deals with several requirements. Firstly, the UAV is dedicated to transferring signals to IoT users belonging to a cluster and the UAV is equipped with N antennas. Secondly, interference among devices in a cluster must be reduced. To this end, the system aims to guarantee the reduced latency required by the system with the specific group of NOMA IoT users connected to the UAV.[1] As a possible solution, these M devices could be divided into different orthogonal groups with benefit from the mobility capability of UAVs, i.e. each group contains two IoT users, D_1, D_2.[2] In this scenario, the UAV-mounted transmitter utilizes the same time-frequency resource to simultaneously transmit the superimposed signals to IoT users by appropriately allocating its transmit power (i.e., power-domain NOMA). We assume a multiple-antenna UAV design and single-antenna ground users motivated by the small size of IoT users. The UAV continuously flies and its movements are characterized by a set of parameters such as constant velocity v, a circular trajectory of radius r and altitude h. Hereby, we assume that the ground users D_1 and D_2 are located at D_1 $(L, 0, 0)$ and D_2 $(-L, 0, 0)$, respectively. We denote φ as the angle of the circle of UAV location, then the location of UAV R is represented as $R(rcos\varphi, rsin\varphi, h)$. It is noted that the IoT users are normally placed at the ground and hence their altitude is zero. After the UAV serves a dedicated cluster, it can move to other clusters. When we focus on the performance analysis of a cluster, Euclidean distances from the ground users D_1, D_2 to the UAV, R, can be calculated, respectively as [39]

$$d_1 = \sqrt{h^2 + r^2 + L^2 - 2rL\cos\varphi}, \tag{2a}$$

$$d_2 = \sqrt{h^2 + r^2 + L^2 + 2rL\cos\varphi}. \tag{2b}$$

We assume that the Rician fading of the channel between the UAV and terrestrial users is based on the probabilistic LoS and non-LoS (NLoS) model, which is affected by the density of the buildings and the distance between the UAV and users. The probability of any user experiencing a LoS

[1] A brute force search algorithm can be deployed to perform user clustering and to maximize the overall spectral efficiency and user fairness subject to satisfying quality of service as well as the total transmit power constraints. The explicit procedures of user clustering is beyond the scope of our paper, and detailed procedures can refer to [38].

[2] We prefer to design a smaller group containing only two IoT users due to high complexity of SIC and worse performance with multiple users in NOMA systems. On the other hand, a two-device NOMA setting has been standardized in the 3GPP in Release 15 [30]. The work in [19] presented similar system model and confirmed that UAV works well with this users arrangement related to satisfaction of performance metrics such as outage probability.

link is represented as [40]:

$$P_{LoS,k} = \frac{1}{1 + pe^{-q(\theta_k - p)}}, k \in \{1, 2\}, \tag{3}$$

where p and q are constant values depending on the surrounding environment, such as sub-urban, urban, dense-urban and $\theta_k = \arcsin\left(\frac{h}{d_k}\right)$. Obviously, the probability of NLoS is $P_{NLoS,k} = 1 - P_{LoS,k}$.

Without loss of generality, we assume that the channel between the UAV and the ground users is $N \times 1$ channel vector, i.e. $\mathbf{h}_k$ presented as $\mathbf{h}_k \in \mathbb{C}^{N\times 1}$ where $\mathbf{h}_k = \left[h_k^1, \ldots, h_k^n, \ldots, h_k^N\right]^T$ whose elements are the channel coefficients and $[\cdot]^T$ denotes the transpose operator. We denote transmit power of the UAV by P. The channel state information (CSI) is assumed to be perfect at each terminal.[3]

During this phase, the UAV simultaneously transmits the normalized information signal $\tilde{x}_1$ and $\tilde{x}_2$ to D_1 and D_2, respectively. The corresponding received signal at D_k can be expressed as [14]:

$$y_{D_k} = \mathbf{h}_k \sqrt{d_k^{-\alpha} L_k} \left(\sqrt{P\varpi_1}\tilde{x}_1 + \sqrt{P\varpi_2}\tilde{x}_2 + \tilde{\eta}_D\right) + n_{D_k}, k \in \{1, 2\}, \tag{4}$$

where ϖ_1 and ϖ_2 represent the fractions of the allocated power to D_1 and D_2, respectively, with the following constraint: $\varpi_1 + \varpi_2 = 1$ and $\varpi_2 > \varpi_1$.[4] It is noted that $\tilde{x}_1 \sim \mathcal{CN}(0, 1)$ and $\tilde{x}_2 \sim \mathcal{CN}(0, 1)$ are the messages dedicated to D_1 and D_2, respectively, α is the path loss exponent, $\tilde{\eta}_D$ is the distortion noise due to imperfect hardware at the UAV, i.e. $\tilde{\eta}_D \sim \mathcal{CN}\left(0, \kappa_{D_1}^2 \varpi_1 P + \kappa_{D_2}^2 \varpi_2 P\right)$ [42], $\kappa_{D_1}^2$ and $\kappa_{D_2}^2$ present the hardware noise level for the transmitted signal at D_k, respectively, $L_k = \left(P_{LoS,k} + \upsilon P_{NLoS,k}\right)$ in which υ denotes the additional attenuation factor of NLoS transmission, and $n_{D_k} \sim \mathcal{CN}(0, I_N N_0)$ is the additive complex white Gaussian noise (AWGN) in which I_N represents the $1 \times N$ identity matrix.

According to NOMA cooperation principle, D_1 detects $\tilde{x}_2$ having strong signal power first while treating $\tilde{x}_1$ as noise, then decodes $\tilde{x}_1$ by using the SIC algorithm to subtract $\tilde{x}_2$. Therefore, with the help of (4), the signal-to-interference-plus-noise-and-distortion ratio (SINDR) at D_1 for signal $\tilde{x}_2$ can be written as:

$$\tilde{\gamma}_{D_1,x_2} = \frac{\varpi_2 P d_1^{-\alpha} L_1 \gamma_1}{P d_1^{-\alpha} L_1 \gamma_1 \left[\kappa_{D_2}^2 \varpi_2 + \left(1 + \kappa_{D_1}^2\right)\varpi_1\right] + N_0} = \frac{\varpi_2 \rho d_1^{-\alpha} L_1 \gamma_1}{\rho d_1^{-\alpha} L_1 \gamma_1 \left[\kappa_{D_2}^2 \varpi_2 + \left(1 + \kappa_{D_1}^2\right)\varpi_1\right] + 1}, \tag{5}$$

where $\gamma_1 \triangleq \|\mathbf{h}_1\|^2$ with $\|.\|$ denotes the Euclidean norm of a vector, $\rho = P/N_0$ is the average signal-to-noise ratio (SNR) at the UAV.

The signal-to-noise-and-distortion ratio (SNDR) of decoding $\tilde{x}_1$ at D_1 can be given as

$$\tilde{\gamma}_{D_1,x_1} = \frac{\varpi_1 \rho d_1^{-\alpha} L_1 \gamma_1}{\rho d_1^{-\alpha} L_1 \gamma_1 \left[\kappa_{D_2}^2 \varpi_2 + \kappa_{D_1}^2 \varpi_1\right] + 1}. \tag{6}$$

Next, D_2 can detect $\tilde{x}_2$ by treating $\tilde{x}_1$ as a noise, the received SINDR at D_2 is given by

$$\tilde{\gamma}_{D_2,x_2} = \frac{\varpi_2 \rho d_2^{-\alpha} L_2 \gamma_2}{\rho d_2^{-\alpha} L_2 \gamma_2 \left[\kappa_{D_2}^2 \varpi_2 + \left(1 + \kappa_{D_1}^2\right)\varpi_1\right] + 1}, \tag{7}$$

where $\gamma_2 \triangleq \|\mathbf{h}_2\|^2$.

III. PERFORMANCE ANALYSIS

In order to investigate the system performance, we first obtain the statistical property of the UAV links.

A. CHANNEL MODEL

The wireless channels between the UAV and the ground users are assumed to experience small-scale fading and large-scale path loss. In general, a UAV-ground link is characterized by the presence of a strong line-of-sight (LoS) path. Therefore, the Rician distribution is an appropriate choice for the UAV-to-ground channel comprised of LoS and multipath scatterers at the ground station receiver [43]. By definition, the probability distribution function (PDF) of the unordered squared channel gain $\gamma_i, i \in \{1, 2\}$ is given by a non-central chi-square distribution with two degrees-of-freedom as [44]:

$$f_{|h_i|^2}(x) = \phi_i e^{-K_i} e^{-\phi_i x} I_0\left(2\sqrt{K_i \phi_i x}\right), \tag{8}$$

where $\phi_i = (1 + K_i)/\Omega_i$, $I_0(x)$ is the zeroth-order modified Bessel function of the first kind, $K_i \triangleq |\mu_i|^2/2\sigma^2$ is the Rician factor and $\Omega_i = \mathbb{E}\left\{|\gamma_i|^2\right\} = 1$ is the normalized average fading power.

Furthermore, we can use the following expression for the density of the sum of N squared i.i.d. Rician random variables, $\gamma_i = \sum_{n=1}^{N} |h_{i,n}|^2, i \in \{1, 2\}$ which is given by [45, Eq. (10)]

$$f_{|\gamma_i|^2}(x) = \phi_i e^{-NK_i} \left(\frac{\phi_i}{NK_i}\right)^{\frac{N-1}{2}} x^{\frac{N-1}{2}} e^{-\phi_i x} \times I_{N-1}\left(2\sqrt{NK_i\phi_i x}\right), \tag{9}$$

with $\Gamma(x)$ is the gamma function.

[3]The channels between the UAV and the ground devices are mostly characterized by time-selective fading since the UAV's mobility leads to the Doppler spread affecting the wireless connections. To detect received signals, the ground users estimate the channel coefficients though pilot signals. The imperfect CSI is usually modeled as an additional complex Gaussian noise and is described in [4].

[4]The decoding order of NOMA devices are decided by considering distances from the devices to the UAV, meaning that transmit power is allocated to the users in a distance-based fashion. The higher power could be allocated for far the IoT device [6], [41].

B. OUTAGE PROBABILITY

When the target rate of the ground users is determined by the quality of service (QoS), the outage probability is an important metric for performance evaluation. We evaluate the outage performance of the two users below.

Firstly, the outage probability at D_1 is given by

$$\begin{aligned}\mathcal{P}_{D_1} &= \Pr\left(\tilde{\gamma}_{D_1,x_2} < \tilde{\varepsilon}_2 \cup \tilde{\gamma}_{D_1,x_1} < \tilde{\varepsilon}_1\right)\\ &= 1 - \Pr\left(\tilde{\gamma}_{D_1,x_2} \geq \tilde{\varepsilon}_2, \tilde{\gamma}_{D_1,x_1} \geq \tilde{\varepsilon}_1\right)\\ &= 1 - \Pr\left(\gamma_1 \geq \tilde{\chi}_{\max}\right), \end{aligned} \tag{10}$$

where $\tilde{\varepsilon}_2 = 2^{R_2} - 1$ with R_2 being the target rate at D_1 to detect x_2, $\tilde{\varepsilon}_1 = 2^{R_1} - 1$ with R_1 being the target rate at D_1 to detect x_2,

$\tilde{\chi}_2 = \frac{\tilde{\varepsilon}_2}{\rho d_1^{-\alpha} L_1 \left\{\varpi_2 - \tilde{\varepsilon}_2\left[\kappa_{D_2}^2 \varpi_2 + \left(1+\kappa_{D_1}^2\right)\varpi_1\right]\right\}}$,

$\tilde{\chi}_1 = \frac{\tilde{\varepsilon}_1}{\rho d_1^{-\alpha} L_1 \left\{\varpi_1 - \tilde{\varepsilon}_1\left[\kappa_{D_2}^2 \varpi_2 + \kappa_{D_1}^2 \varpi_1\right]\right\}}$ and $\tilde{\chi}_{\max} = \max\left(\tilde{\chi}_2, \tilde{\chi}_1\right)$.

Note that (10) is derived on the condition of $\varpi_2 > \tilde{\varepsilon}_2\left[\kappa_{D_2}^2 \varpi_2 + \left(1+\kappa_{D_1}^2\right)\varpi_1\right]$ and $\varpi_1 > \tilde{\varepsilon}_1\left[\kappa_{D_2}^2 \varpi_2 + \kappa_{D_1}^2 \varpi_1\right]$.

Proposition 1: The outage probability at D_1 of a multi-antenna relaying system with Rician fading can be expressed as (11).

$$\mathcal{P}_{D_1} = 1 - \frac{\pi e^{-NK_1}}{(NK_1)^N} \Lambda\left(\frac{1}{NK_1}, \frac{1}{NK_1\phi_1\tilde{\chi}_{\max}}\right). \tag{11}$$

where $\Lambda(x, y)$ is shown on the next top page and $\mathcal{H}_{p,q:u,v:e,f}^{m,n:s,t:i,j}(\cdot)$ represents the extended generalized bivariate Fox H-function (EGBFHF) in [46].

Proof: See Appendix A

Next, the outage probability at D_2 is computed by

$$\begin{aligned}\mathcal{P}_{D_2} &= 1 - \Pr\left(\tilde{\gamma}_{D_2,x_2} \geq \tilde{\varepsilon}_2\right)\\ &= 1 - \Pr\left(\gamma_2 \geq \bar{\chi}_2\right), \end{aligned} \tag{13}$$

where $\bar{\chi}_2 = \frac{\tilde{\varepsilon}_2}{\rho d_2^{-\alpha} L_2 \left\{\varpi_2 - \tilde{\varepsilon}_2\left[\kappa_{D_2}^2 \varpi_2 + \left(1+\kappa_{D_1}^2\right)\varpi_1\right]\right\}}$.

Similar to $\mathcal{P}_{D_1}$, we can show $\mathcal{P}_{D_2}$ is given by

$$\mathcal{P}_{D_2} = 1 - \frac{\pi e^{-NK_2}}{(NK_2)^N} \Lambda\left(\frac{1}{NK_2}, \frac{1}{NK_2\phi_2\bar{\chi}_2}\right). \tag{14}$$

Remark 1: The results in (11) and (14) indicate the power allocation factors, the target rates, and SNR at the UAV are the main contributors to the analysis of the system performance. If the UAV has the capability to learn parameters from environment, the system could improve the performance at each user directly rather than the case that the UAV transmits with fixed system parameters at the downlink.

C. SYSTEM THROUGHPUT

In this section, we move our attention to another system performance metric, namely the throughput. When the codewords are short (i.e., shorther than the coherence time), the throughput could be evaluated prior to the ergodic rate. The system throughput at D_1 and D_2 can be similarly derived as [47]

$$\tau_{sys} = \left(1 - \mathcal{P}_{D_1}\right) R_1 + \left(1 - \mathcal{P}_{D_2}\right) R_2. \tag{15}$$

Remark 2: The result in (15) indicates that very high data rates R_1, R_2 between the UAV and the ground users D_1, D_2 result in a lower successful probability of signal decoding corresponding to a degraded system throughput. In contrast, to enhance the successful decoding probability, lower values of R_1, R_2 are required, but the system throughput cannot be high since the transmission rates R_1, R_2 affect to throughput performance directly; thus, revealing a trade-off.

D. ERGODIC CAPACITY

When the codeword is long enough (i.e., longer than the coherence time), the ergodic rate should be further analyzed, and the ergodic rate performance of two devices can be determined as follows.

The ergodic capacity at D_2 is calculated as

$$\begin{aligned}\tilde{\mathcal{C}}_2 &= \mathbb{E}\left\{\log_2\left(1 + \tilde{\gamma}_{D_2,x_2}\right)\right\}\\ &= \frac{1}{\ln 2}\int_0^{\frac{\bar{\xi}}{\bar{\zeta}}} \frac{1}{1+x}\left[1 - F_{\gamma_2}\left(\frac{x}{\bar{\xi} - \bar{\zeta}x}\right)\right] dx, \end{aligned} \tag{16}$$

where $\bar{\zeta} = \frac{\rho L_2}{d_2^{\alpha}}\left[\kappa_{D_2}^2 \varpi_2 + \left(1+\kappa_{D_1}^2\right)\varpi_1\right]$ and $\bar{\xi} = \frac{\varpi_2 \rho L_2}{d_2^{\alpha}}$.

Proposition 2: The approximate closed-form expression of the ergodic capacity of D_2 is written as

$$\begin{aligned}\widetilde{\mathcal{C}}_2 \approx &\frac{\pi^2 \bar{\xi} e^{-NK_2}}{2T\bar{\zeta}\ln 2 (NK_2)^N} \sum_{t=1}^{T} \frac{\sqrt{1-\varphi_t^2}}{1 + \Theta(\varphi_t)}\\ &\times \Lambda\left(\frac{1}{NK_2}, \frac{\bar{\xi} - \bar{\zeta}\Theta(\varphi_t)}{NK_2\phi_2\Theta(\varphi_t)}\right), \end{aligned} \tag{17}$$

where $\Theta(t) = \frac{\bar{\xi}(t+1)}{2\bar{\zeta}}$ and $\varphi_t = \cos\left(\frac{2t-1}{2T}\pi\right)$.

Proof: See Appendix B.

Next, the ergodic capacity at D_1 is given as

$$\begin{aligned}\tilde{\mathcal{C}}_1 &= \mathbb{E}\left\{\log_2\left(1 + \tilde{\gamma}_{D_1,x_1}\right)\right\}\\ &= \frac{1}{\ln 2}\int_0^{\frac{\tilde{\xi}}{\tilde{\zeta}}} \frac{1}{1+x}\left[1 - F_{\gamma_1}\left(\frac{x}{\tilde{\xi} - \tilde{\zeta}x}\right)\right] dx, \end{aligned} \tag{18}$$

where $\tilde{\xi} = \rho d_1^{-\alpha}\varpi_1$ and $\tilde{\zeta} = \rho d_1^{-\alpha}\left[\kappa_{D_2}^2 \varpi_2 + \kappa_{D_1}^2 \varpi_1\right]$.

$$\Lambda(x, y) = \mathcal{H}_{3,1:0,1:1,1}^{0,1:1,0:0,1}\left(\begin{matrix}(1-N;1,1),(0;1,1),(0.5-N;1,1)\\(0.5-N;1,1)\end{matrix}\middle|\begin{matrix}-\\(0,1)\end{matrix}\middle|\begin{matrix}(1,1)\\(0,1)\end{matrix}\middle| x, y\right). \tag{12}$$

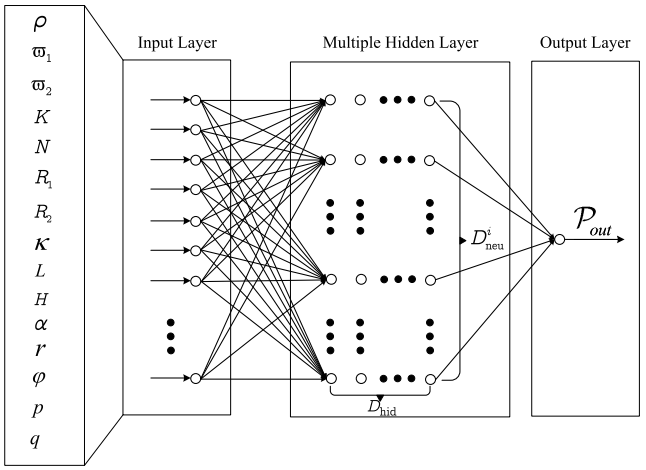

FIGURE 2. A design of DNN used to predict the system performance.

By replacing new variable $x = \frac{\tilde{\xi}}{2\tilde{\zeta}}(t+1)$ and using Gaussian-Chebyshev quadrature [52, Eq. (25.4.38)], an approximate closed-form ergodic capacity at D_2 can be obtained by

$$\widetilde{\mathcal{C}}_1 \approx \frac{\pi^2 \tilde{\xi} e^{-NK_1}}{2R\tilde{\zeta}\ln 2 (NK_1)^N} \sum_{r=1}^{R} \frac{\sqrt{1-\varphi_r^2}}{1+\Xi(\varphi_r)} \times \Lambda\left(\frac{1}{NK_1}, \frac{\bar{\xi} - \bar{\zeta}\Xi(\varphi_r)}{NK_1\phi_1\Xi(\varphi_r)}\right), \quad (19)$$

where $\Xi(t) = \frac{\tilde{\xi}}{2\tilde{\zeta}}(t+1)$ and $\varphi_r = \cos\left(\frac{2r-1}{2R}\pi\right)$.

Remark 3: The results of the system performance evaluations in (11), (14), (17) and (19) are very important to UAV to direct such UAV flies close to or far way from the ground users D_1, D_2 with respect to satisfy data requirements for each user. In [19], the throughput of the first user in a cluster can be maximized after guaranteeing the desired throughput for the second user since such throughput depends on power allocation coefficients and target symbol rates. However, the UAV finds hard to know throughput performance to conducting an optimization at the time that it transmits signals. To this end, this paper introduces DNN in the next section as a new way to predict performance for ground users.

IV. DNN-BASED PERFORMANCE PREDICTION

A. THE STRUCTURE OF THE DNN

The DNN is a feed-forward neural network, which can be deployed at the UAV. Figure 2 depicts the DNN including one output layer, one input layer, and multiple hidden layers, i.e. D_{hid} layers. The parameters collected to the UAV correspond to 15 neurons, and these primary system parameter settings are given in Table 2. The output layer with one neuron corresponds to the expected outage performance. The linear and activation functions are used to obtain the predicted outage probability $\mathcal{P}_{out}$ [29], [48]. The rectified linear unit (ReLU) function in this case can be applied as an activation function. It is noted that single hidden layer i contains $D^i_{neu}, i = 1, \ldots, D_{hid}$ neurons.

TABLE 2. Inputs for DNN testing and training.

Inputs	Values	Inputs	Values
ρ	[-5:5:25]	κ	0.01
ϖ_1	0.1	L	2
ϖ_2	0.9	H	10
K	2	α	2
N	[1,2]	r	0.1
R_1	0.75	φ	45
R_2	0.75	$\{p, q\}$	$\{4.886, 0.429\}$

It is assumed that the training phase is performed offline to reduce the computational complexity, and the implementation cost can be decreased accordingly. In particular, the training process can be conducted in two phases corresponding to the training and prediction ones. The adaptive moment estimation (Adam) optimization algorithm can be deployed in the training phase since the network can learn input-output relations offline. As a result, the model parameters can be optimized based on the dataset. The system can update weights during the backpropagation procedure when computing the loss function. It would be a simpler procedure when this phase is performed one time and then reused several times to predict outage behavior for the communication between the UAV and IoT users. After the offline training model is finished, the achieved results can be leveraged to obtain an online prediction of the outage probability.

B. DATASET

The UAV can be initialized by collecting system parameters for its input layer with the size of 1×15. In a practical scenario, the UAV can accumulate the dataset over a long period of time. However, the number of samples used for simulation in this paper is sufficient to obtain high accurate predictions for outage performance. In particular, the dataset contains i samples of the collected data from the server where the UAV can be connected to, i.e. input-output relationship could be $Data[i] = \left[t[i], \mathcal{P}^i_{D_j}\right]$, where $j \in \{1, 2\}$ and $t[i]$ is a feature vector that corresponds to the parameters listed in Table 2. In this study, the UAV can process 10^5 samples, i.e., $Data[i], i = 1, 2, \ldots, 10^5$. The system can also divide data into portions including the training set, $\wp_{trn}$, validation set, $\wp_{val}$, and test set, $\wp_{tes}$ (corresponding to three groups 80%, 10%, and 10% of data resource, respectively).

The exactness of such prediction can be evaluated via the MSE, i.e., $MSE = \frac{1}{|\wp_{tes}|}\sum_{i=0}^{|\wp_{tes}|-1}\left(\mathcal{P}_{out} - \mathcal{P}^{tes}_{out}\right)^2$ in [29] and [48]. The DNN can work effectively as long as the UAV is able to determine $RMSE = \sqrt{MSE}$ as the acceptable value. It is noted that such an error can be propagated back through the DNN to gradually adjust the weights and biases. Next, we present Algorithm 1 to determine the main steps required for training and evaluating a DNN [29], [48].

C. REAL-TIME PREDICTION

Following the offline training, the resulting DNN model with weights and biases may be represented as in a compact mapping function i.e. $\mathbb{J}(\cdot)$. When the new network data is

Algorithm 1 Procedures for the DNN: Training and Testing

Input : The system parameters; Installation for DNN: $D_{hih} = 5$, $D^{i}_{neu} = 128$, $RMSE_{th} = 2 \times 10^{-2}$ and learning rate $lr = 10^{-3}$

Output: A trained DNN

begin

Extracting from dataset for $\wp_{trn}$, $\wp_{val}$, and $\wp_{tes}$

Perform DNN relying on Keras and TensorFlow

while ($RMSE \geq RMSE_{th}$) **do**

Changing D_{hih}, D^{i}_{neu}, lr, and the number of epochs dynamically

Using S_{trn} and S_{val} for training procedure and save them in the validated DNN (validatedDNN.h5)

Obtaining RMSE when set S_{tes} into validatedDNN.h5.

end

return *trainedDNN.h5 data*

end

organized as a new vector (x_{new}), the outcome of the DNN model may be expressed as

$$\mathcal{P}^{pred}_{out} = \mathbb{J}\left(x_{new}\right). \tag{20}$$

From (20), the outage performance can be predicted by the resulting DNN mode in a short execution time. Since the DNN's capacity may be improved by including additional hidden layers or more neurons/hidden unit networks, the parameters of the DNN can be adaptively built to obtain the lowest error throughout the training process.

V. NUMERICAL RESULTS AND DISCUSSIONS

In this section, we present the numerical and simulation results to examine the performance of both NOMA-aided and OMA-aided UAV. For summarize the main simulation parameters in Table 3 (unless otherwise stated). Note that we set $\kappa = \kappa^2_{D_1} = \kappa^2_{D_2}$, $K = K_1 = K_2$ and consider the scenario in sub-urban environment. The derived mathematical expressions are verified to confirm exactness of proposed expressions. In all simulation results, we denote "ana.", "sim." for analytical and simulation results respectively.

Figure 3 shows the training and validation versus epochs. As can be observed, the training's correctness can be obtained after 30 epochs. In addition, MSE is lower than 10^{-5} after 40 epochs. It means that the estimated OP is tightly close to the test data. Next, we compare the execution time of the Monte Carlo simulation, analytical, and DNN model for the proposed system. Table 4 shows the execution time, which means the time spent assessing outage performance. As can be observed, the suggested DNN model takes the least amount of time to execute the three alternatives. Thus, the proposed DNN emerges as an excellent tool for evaluating real-time outage performance.

TABLE 3. Simulation Parameters.

Parameters	Value
The iteration number of the Monte Carlo simulation	10^7
The target rate	$R_1 = 0.75$ & $R_2 = 0.75$
The power allocation coefficient	$\varpi_2 = 0.9$ & $\varpi_1 = 0.1$
The hardware noise level	$\kappa = \kappa^2_{D_1} = \kappa^2_{D_1} = 0.01$
The path loss factor	$\alpha = 2$
The altitude of the UAV	$h = 10$
The circular trajectory of the radius	$r = 0.1$
The location of the ground users	$L = 2$
The angle of the circle of UAV location	$\varphi = 45$
Additional attenuation factor	$\upsilon = 20$ (dB)
Environment parameter	$p = 4.886$
Environment parameter	$q = 0.429$

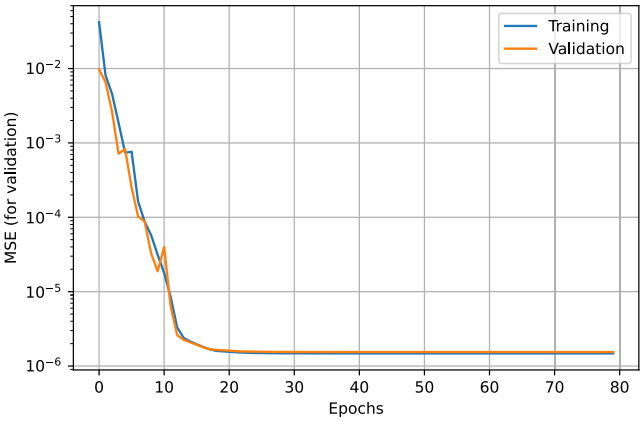

FIGURE 3. The MSE's convergence in validating and training the DNN.

TABLE 4. The execution time.

Approaches	Monter Carlo Simulation	Analytical	DNN model
Execution time	1.2 s	27.13 s	0.41 s

Figure 4 depicts the outage probability versus the average transmit SNR at the UAV under different Rician fading parameter K. As the first observation, when the quality of channels can be improved, an increasing Rician-K coefficient results in performance improvements. For the case with $K = 5$, the second device is determined as the best one among three considered cases of $K = 1, 3, 5$ and hence, strong channels support stable transmission. To confirm the correctness of the analytical expression, we run both numerical and analytical results obtained from (11) and (14). We observe that the theoretical computation and Monte Carlo simulation match. The main reason is that increasing the Rician-K factor yields in higher SINDR providing a better outage behavior since the channel quality of the considered system improves.

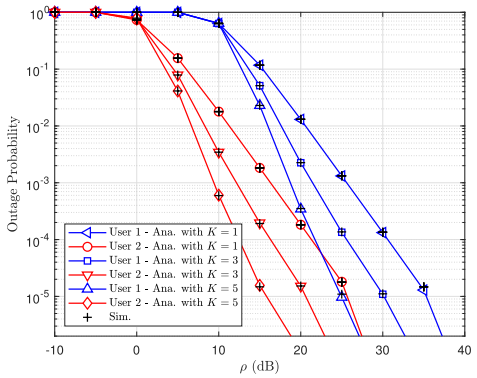

FIGURE 4. Outage probability of D_1 and D_2 versus SNR and different values of K.

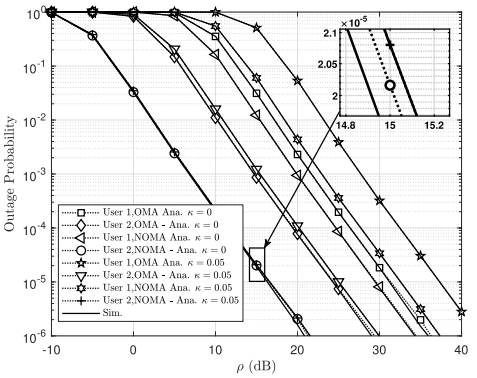

FIGURE 6. Outage probability of D_1 and D_2 versus SNR with $R_1 = 1$, $R_2 = 0.5$ and $N = K = 2$.

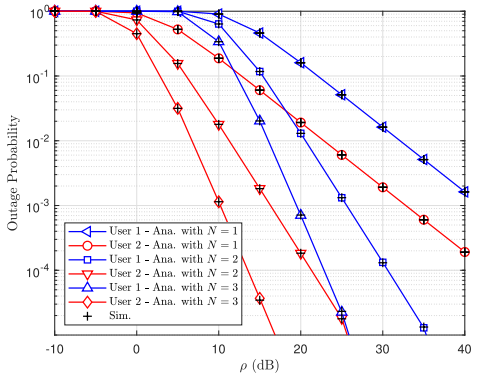

FIGURE 5. Outage probability of D_1 and D_2 versus SNR at the UAV with different number of antennas N, with $K = 2$.

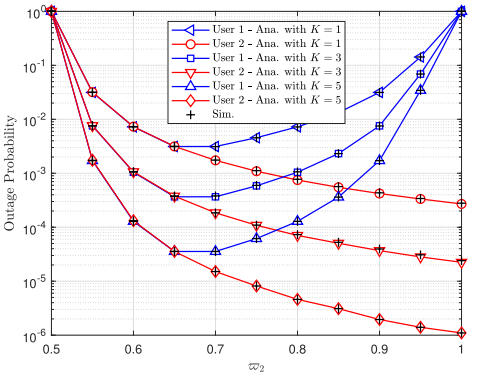

FIGURE 7. Outage probability of D_1 and D_2 versus ϖ_2 with $R_1 = R_2 = 1$, $\kappa = 0.01$ and $\rho = 15$ (dB).

Figure 5 illustrates the impact of the number of transmit antennas at the UAV, N, on the outage probability. The higher number of antennas at the UAV, the better the outage probability. It can also be seen that the outage behavior of the second device is better than that of the first device since higher power is allocated to the second device ($\varpi_2 = 0.9$). This result confirms that adding more antennas at the UAV leads to an increase in spatial degrees-of-freedom at the receivers and further improves the outage performance. The slopes of the curves is proportional to the number of antennas. They reflect the diversity gain of the system.

Figure 6 demonstrates the outage probability versus the average SNR at the UAV considering ideal and non-ideal conditions with hardware at the UAV. We can see the outage curves for two cases of hardware imperfection, i.e. $\kappa = 0$ and $\kappa = 0.05$, to characterize the impact of imperfect hardware level to NOMA and OMA approaches. We observe that the outage probability of two IoT users become worse as the value of parameters of κ increases. It can be concluded that the outage probability of considered systems is limited by the level of hardware imperfection. In addition, the gap between the outage probability of NOMA and OMA cases becomes large at higher level of hardware noise $\kappa = 0.05$.

Figure 7 depicts the impact of the power allocation coefficients on the performance of two IoT devices. This case corresponds to hardware noise $\kappa = 0.01$. We observe that the outage probability of the first device reaches the lowest point as $\varpi_2 = 0.65$ regardless of value of K. This implies that the power allocation coefficients play a crucial role in the outage behavior rather than any other parameters. We also confirm that higher power assigned to the second device benefits its performance while this allocation harms the performance at the first device. The worse performance at the first device become significant when ϖ_2 goes from 0.7 to 1. This can be explained as follows: detecting the signal at the first device depends on how large SINDR in (6) is. Since ϖ_2 becomes smaller, value of SINDR in (6) results in a worse outage performance.

Figure 8 illustrates the outage performance of the proposed UAV-based IoT system versus the location of the UAV for two IoT users. It is assumed that the UAV maintains hardware noise at $\kappa = 0.01$. We can see that, at $\varphi = 0$, the outage probability of the first user is minimum. This is due to the fact that when the UAV stays close to the users, the performance would be best. We note that when r is small, changing values of φ does not affect the performance much. It is because r reflect moving area of the UAV, so small r means smaller change in the location of the UAV. That lead to small variation in the OP.

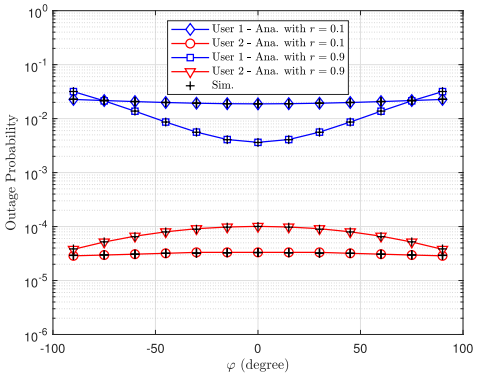

FIGURE 8. Outage probability of D_1 and D_2 versus φ with $\varpi_2 = 0.95$, $\varpi_1 = 0.05$, $R_1 = R_2 = 1$, $\kappa = 0.01$, $N = K = 2$ and $\rho = 5$ (dB).

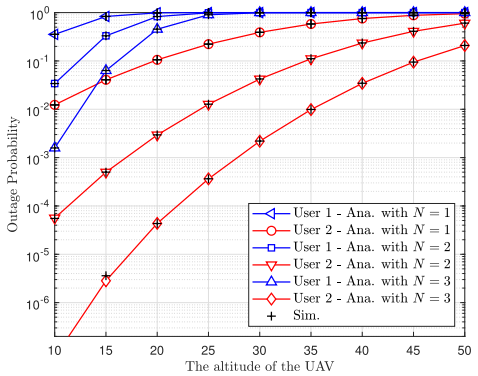

FIGURE 9. The outage probability with ideal target rate of different UAV altitude in which $\varpi_2 = 0.9$, $\varpi_1 = 0.1$, $\kappa = 0.01$ and $K = 4$.

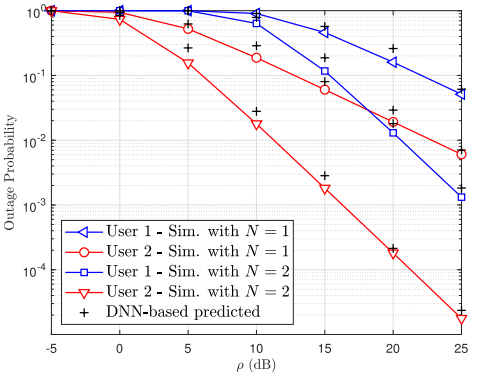

FIGURE 10. Comparison between the predicted outage performance and analytical simulation under different N.

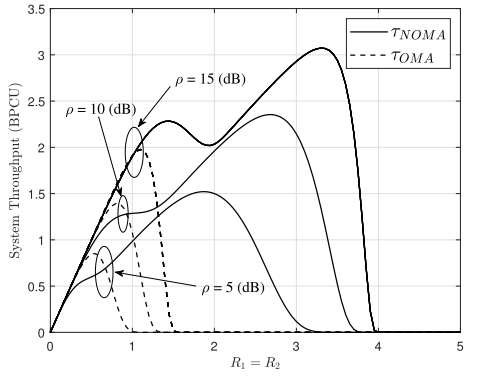

FIGURE 11. System throughput at D_1 and D_2 versus $R_i, i \in \{1, 2\}$ with $\varpi_2 = 0.95$, $\varpi_1 = 0.05$, $\kappa = 0.01$ and $N = K = 2$.

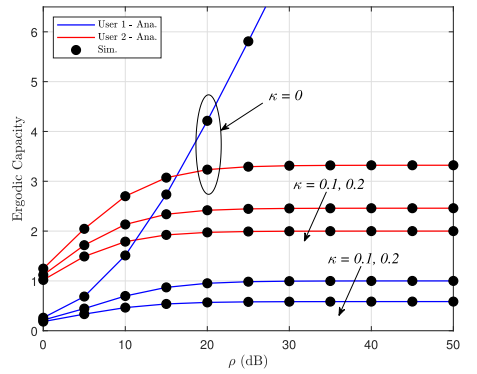

FIGURE 12. The ergodic capacity versus SNR with $N = K = 2$ and $r = 0.9$.

Figure 9 presents the outage behavior of two IoT users versus the altitude h of the UAV for different setting of transmit antennas at the UAV. We observe that the outage performance of both two users become worse when UAV's altitude is higher. This means that when the UAV flies low enough to closely meet the users, the outage performance can be satisfied. Moreover, the gap between the outage probabilities of User 1 and User 2 is remarkable when the UAV is at low altitude, but is smaller when h is large. This can be explained as follows: increasing the altitude of UAV leads to an increase in the probability of having LoS link, resulting in a lower SINDR corresponding to a worse outage probability.

Figure 10 demonstrates how DNN can predict the outage performance of the two users. We observe that the predicted values of the outage behavior are close to outage probabilities obtained by Monte-Carlo and analytical simulation. Since the outage performance of the two users depend on how the UAV allocates transmit power to their signals, the UAV can predict outage behavior of two users and adjust power allocation factors to satisfy the fairness or other requirements at the users.

Figure 11 depicts the throughput performance of two users versus the target rates. Since the target rates R_1, R_2 limit outage performance, an increase in the target rates leads to a decrease in throughput. Thus, the UAV-NOMA system is sensitive to data rates requirements as throughput becomes worse at the higher target rates.

Figure 12 illustrates the ergodic capacity of the two users versus the SNR at the UAV. At lower range of SNR, the ergodic capacity of the considered system can be enhanced when the quality of received signal becomes better. Unfortunately, when the SNR goes beyond 20 dB, the ergodic capacity cannot be enhanced due to hardware noise. It is worth noting that the first user can increase the ergodic capacity significantly in the ideal condition of hardware $\kappa =$

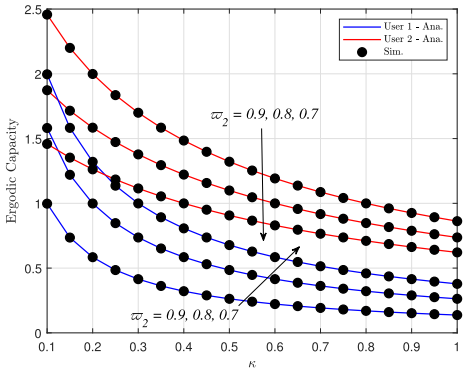

FIGURE 13. The ergodic capacity versus κ with $N = 3$, $K = 10$, $r = 0.1$ and $\rho = 30$ (dB).

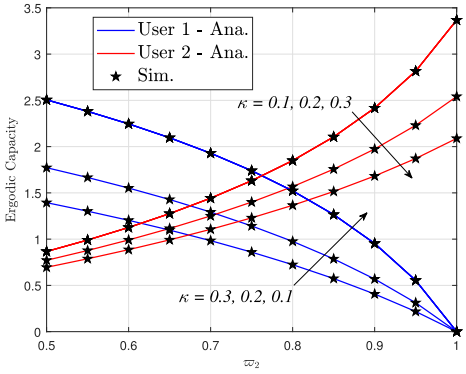

FIGURE 14. The ergodic capacity versus ϖ_2 with $N = K = 2$, $r = 0.9$ and $\rho = 20$ (dB).

0. Figure 13 also confirms levels of hardware noise make a crucial impact on the ergodic capacity of both users regardless of any change to power allocation coefficients.

Finally, Figure 14 confirms that if the system can be determined suitable power allocation factor ϖ_2, the ergodic performance of two users showcases their optimal values concurrently. This result also demonstrates that as more power is assigned to the second users, the ergodic capacity increases, which benefits the system.

VI. CONCLUSION

We have presented and provided performance analysis of an UAV-NOMA IoT system with residual hardware noise enhanced by a DNN approach to exhibit a new way to allow flying BSs predict the performance of the IoT users. In particular, we provided closed-form expressions for evaluating the system performance including the outage probability, the throughput, and the ergodic capacity. The simulation results indicate that outage, throughput, and ergodic capacity performance of the two users in a cluster mostly depends on power allocation factors, hardware noise level, and date rates. In addition, the maximum throughput for the UAV-NOMA is always superior to that of the benchmark (UAV-OMA system). Further, we highlighted in the simulation that the benefits of DNN and user arrangement (many clusters associated with OMA scheme while NOMA signalling is used for users in each cluster) over conventional methods. To deal with unpredictable performance at ground users, the UAV can leverage a DNN to predict the user performance and adjust parameters to satisfy the fairness and quality of service at each user.

APPENDIX A
PROOF OF PROPOSITION 1

By replacing (9) in (10), the outage probability at D_1 can be calculated as

$$\begin{aligned}\mathcal{P}_{D_1} &= 1 - \Pr\left(\gamma_1 \geq \tilde{\chi}_{\max}\right) \\ &= 1 - \phi_i e^{-NK_i}\left(\frac{\phi_i}{NK_i}\right)^{\frac{N-1}{2}} \int_{\tilde{\chi}_{\max}}^{\infty} x^{\frac{N-1}{2}} \\ &\quad \times e^{-\phi_i x} I_{N-1}\left(2\sqrt{NK_i\phi_i x}\right) dx \\ &= 1 - \phi_i e^{-NK_i}\left(\frac{\phi_i}{NK_i}\right)^{\frac{N-1}{2}} \int_{0}^{\infty} H\left(\frac{x}{\tilde{\chi}_{\max}} - 1\right) \\ &\quad \times x^{\frac{N-1}{2}} e^{-\phi_i x} I_{N-1}\left(2\sqrt{NK_i\phi_i x}\right) dx, \end{aligned} \tag{21}$$

where $H(x)$ is unit step function as $H(x) = \begin{cases} 1, x > 0 \\ 0, x < 0 \end{cases}$.

To solve the integrals in $\mathcal{P}_{D_1}$, we utilize the following transformations involving the Meijer G-function [53]

$$H(1 - |x|) = G_{1,1}^{1,0}\left(x \middle| \begin{matrix} 1 \\ 0 \end{matrix}\right), \tag{22}$$

$$H(|x| - 1) = G_{1,1}^{0,1}\left(x \middle| \begin{matrix} 1 \\ 0 \end{matrix}\right), \tag{23}$$

$$e^{-ax} = G_{0,1}^{1,0}\left(ax \middle| \begin{matrix} - \\ 0 \end{matrix}\right), \tag{24}$$

$$I_v(x) = \pi 2^{-v} x^v G_{1,3}^{1,0}\left(\frac{x^2}{4} \middle| \begin{matrix} 0.5 \\ 0, -v, 0.5 \end{matrix}\right), \tag{25}$$

By expressing the relevant functions in (21) into Meijer G-function using the above equalities in (22), (24) and (25), $\mathcal{P}_{D_1}$ is expressed as

$$\begin{aligned}\mathcal{P}_{D_1} &= 1 - \pi\phi_i^N e^{-NK_i} \int_{0}^{\infty} x^{N-1} G_{0,1}^{1,0}\left(\phi_i x \middle| \begin{matrix} - \\ 0 \end{matrix}\right) \\ &\quad \times G_{1,3}^{1,0}\left(NK_i\phi_i x \middle| \begin{matrix} 0.5 \\ 0, 1-N, 0.5 \end{matrix}\right) G_{1,1}^{0,1}\left(\frac{x}{\tilde{\chi}_{\max}} \middle| \begin{matrix} 1 \\ 0 \end{matrix}\right) dx. \end{aligned} \tag{26}$$

We apply the following (27), as shown at the top of the next page, to solve integrals (26) in which $H_{p,q:u,v:e,f}^{m,n:s,t:i,j}(\cdot)$ stands for the extended generalized bivariate Fox H-function (EGBFHF) in [46]. This function can be conveniently evaluated using mathematical software such as Mathematica [50, Table 1] and Matlab [51, Appx A].

$$\int_0^\infty x^{\lambda-1} G_{p,q}^{m,0}\left(\eta x \left| \begin{matrix} \mathbf{a}_p \\ \mathbf{b}_q \end{matrix}\right.\right) G_{p_2,q_2}^{m_2,n_2}\left(\theta x^h \left| \begin{matrix} \mathbf{c}_{p_2} \\ \mathbf{d}_{q_2} \end{matrix}\right.\right) G_{p_3,q_3}^{m_3,n_3}\left(\delta x^k \left| \begin{matrix} \mathbf{e}_{p_3} \\ \mathbf{f}_{q_3} \end{matrix}\right.\right) dx = \eta^{-\lambda}$$
$$\times H_{q,p:p_2,q_2:p_3,q_3}^{0,m:m_2,n_2:m_3,n_3}\left(\begin{matrix} (1-\mathbf{b}_q-\lambda;h,k) \\ (1-\mathbf{a}_p-\lambda;h,k) \end{matrix} \middle| \begin{matrix} (\mathbf{c}_{p_2},1) \\ (\mathbf{d}_{q_2},1) \end{matrix} \middle| \begin{matrix} (\mathbf{e}_{p_3},1) \\ (\mathbf{f}_{q_3},1) \end{matrix} \middle| \frac{\theta}{\eta^h}, \frac{\delta}{\eta^k} \right). \quad (27)$$

Base on (27), the outage probability of D_1 is written as

$$\mathcal{P}_{D_1} = 1 - \frac{\pi e^{-NK_i}}{(NK_i)^N} \Lambda\left(\frac{1}{NK_1}, \frac{1}{NK_1\phi_1\tilde{\chi}_{\max}}\right), \quad (28)$$

where $\Lambda(x, y)$ is specified by (12),

This completes the proof.

APPENDIX B
PROOF OF PROPOSITION 2

Considering on (16), putting $t = \frac{2\bar{\zeta}x}{\bar{\xi}} - 1$ and it means that $\frac{\bar{\xi}(t+1)}{2\bar{\zeta}} = x$. Then, we have $\frac{\bar{\xi}}{2\bar{\zeta}}dt = dx$, (29) can be achieved as

$$\widetilde{\mathcal{C}}_2 = \frac{\pi\bar{\xi}e^{-NK_2}}{2\bar{\zeta}\ln 2(NK_2)^N} \int_{-1}^{1} \frac{1}{1+\Theta(t)} \times \Lambda\left(\frac{1}{NK_2}, \frac{\bar{\xi}-\bar{\zeta}\Theta(t)}{NK_2\phi_2\Theta(t)}\right) dt. \quad (29)$$

It is not easy to derive a closed-form expression for (29), thus, we aim for an accurate approximation. By using Gaussian-chebyshev quadrature [52, Eq. (25.4.38)], we have $\tilde{\mathcal{C}}_2$ is given by

$$\widetilde{\mathcal{C}}_2 \approx \frac{\pi^2\bar{\xi}e^{-NK_2}}{2T\bar{\zeta}\ln 2(NK_2)^N} \sum_{t=1}^{T} \frac{\sqrt{1-\varphi_t^2}}{1+\Theta(\varphi_t)} \times \Lambda\left(\frac{1}{NK_2}, \frac{\bar{\xi}-\bar{\zeta}\Theta(\varphi_t)}{NK_2\phi_2\Theta(\varphi_t)}\right), \quad (30)$$

where $\Theta(t) = \frac{\bar{\xi}(t+1)}{2\bar{\zeta}}$ and $\varphi_t = \cos\left(\frac{2t-1}{2T}\pi\right)$.

This completes the proof.

REFERENCES

[1] J. Liu, Y. Shi, Z. Md. Fadlullah, and N. Kato, "Space-air-ground integrated network: A survey," *IEEE Commun. Surveys Tuts.*, vol. 20, no. 4, pp. 2714–2741, 4th Quart., 2018.

[2] R. Chen, Y. Sun, L. Liang, and W. Cheng, "Joint power allocation and placement scheme for UAV-assisted IoT with QoS guarantee," *IEEE Trans. Veh. Technol.*, vol. 71, no. 1, pp. 1066–1071, Jan. 2022.

[3] A. Fotouhi, H. Qiang, M. Ding, M. Hassan, L. G. Giordano, A. Garcia-Rodriguez, and J. Yuan, "Survey on UAV cellular communications: Practical aspects, standardization advancements, regulation, and security challenges," *IEEE Commun. Surveys Tuts.*, vol. 21, no. 4, pp. 3417–3442, 4th Quart., 2019.

[4] T. M. Hoang, L. T. Dung, B. C. Nguyen, X. H. Le, X. N. Tran, and T. Kim, "Outage probability and throughput of mobile multiantenna UAV-assisted FD-NOMA relay system with imperfect CSI," *IEEE Syst. J.*, vol. 17, no. 1, pp. 1477–1488, Mar. 2023.

[5] L. Zhao, K. Yang, Z. Tan, X. Li, S. Sharma, and Z. Liu, "A novel cost optimization strategy for SDN-enabled UAV-assisted vehicular computation offloading," *IEEE Trans. Intell. Transp. Syst.*, vol. 22, no. 6, pp. 3664–3674, Jun. 2021.

[6] D.-T. Do, A.-T. Le, Y. Liu, and A. Jamalipour, "User grouping and energy harvesting in UAV-NOMA system with AF/DF relaying," *IEEE Trans. Veh. Technol.*, vol. 70, no. 11, pp. 11855–11868, Nov. 2021.

[7] T. Bao, H. Wang, W.-J. Wang, H.-C. Yang, and M. O. Hasna, "Secrecy outage performance analysis of UAV-assisted relay communication systems with multiple aerial and ground eavesdroppers," *IEEE Trans. Aerosp. Electron. Syst.*, vol. 58, no. 3, pp. 2592–2600, Jun. 2022.

[8] J. Plachy, Z. Becvar, P. Mach, R. Marik, and M. Vondra, "Joint positioning of flying base stations and association of users: evolutionary-based approach," *IEEE Access*, vol. 7, pp. 11454–11463, 2019.

[9] J. Lyu, Y. Zeng, and R. Zhang, "UAV-aided offloading for cellular hotspot," *IEEE Trans. Wireless Commun.*, vol. 17, no. 6, pp. 3988–4001, Jun. 2018.

[10] L. Qu, G. Xu, Z. Zeng, N. Zhang, and Q. Zhang, "UAV-assisted RF/FSO relay system for space-air-ground integrated network: A performance analysis," *IEEE Trans. Wireless Commun.*, vol. 21, no. 8, pp. 6211–6225, Aug. 2022.

[11] S. Mirbolouk, M. Valizadeh, M. C. Amirani, and S. Ali, "Relay selection and power allocation for energy efficiency maximization in hybrid satellite-UAV networks with CoMP-NOMA transmission," *IEEE Trans. Veh. Technol.*, vol. 71, no. 5, pp. 5087–5100, May 2022.

[12] P. K. Singya and M.-S. Alouini, "Performance of UAV-assisted multiuser terrestrial-satellite communication system over mixed FSO/RF channels," *IEEE Trans. Aerosp. Electron. Syst.*, vol. 58, no. 2, pp. 781–796, Apr. 2022.

[13] B. Wang, R. Zhang, C. Chen, X. Cheng, L. Yang, H. Li, and Y. Jin, "Graph-based file dispatching protocol with D2D-enhanced UAV-NOMA communications in large-scale networks," *IEEE Internet Things J.*, vol. 7, no. 9, pp. 8615–8630, Sep. 2020.

[14] X. Li, Q. Wang, Y. Liu, T. A. Tsiftsis, Z. Ding, and A. Nallanathan, "UAV-aided multi-way NOMA networks with residual hardware impairments," *IEEE Wireless Commun. Lett.*, vol. 9, no. 9, pp. 1538–1542, Sep. 2020.

[15] N. Zhao, X. Pang, Z. Li, Y. Chen, F. Li, Z. Ding, and M.-S. Alouini, "Joint trajectory and precoding optimization for UAV-assisted NOMA networks," *IEEE Trans. Commun.*, vol. 67, no. 5, pp. 3723–3735, May 2019.

[16] I. Budhiraja, N. Kumar, S. Tyagi, and S. Tanwar, "Energy consumption minimization scheme for NOMA-based mobile edge computation networks underlaying UAV," *IEEE Syst. J.*, vol. 15, no. 4, pp. 5724–5733, Dec. 2021.

[17] D. Xu, Y. Sun, D. W. K. Ng, and R. Schober, "Multiuser MISO UAV communications in uncertain environments with no-fly zones: Robust trajectory and resource allocation design," *IEEE Trans. Commun.*, vol. 68, no. 5, pp. 3153–3172, May 2020.

[18] B. Liu, Y. Wan, F. Zhou, Q. Wu, and R. Q. Hu, "Robust trajectory and beamforming design for cognitive MISO UAV networks," *IEEE Wireless Commun. Lett.*, vol. 10, no. 2, pp. 396–400, Feb. 2021.

[19] S. K. Singh, K. Agrawal, K. Singh, A. Bansal, C.-P. Li, and Z. Ding, "On the performance of laser-powered UAV-assisted SWIPT enabled multiuser communication network with hybrid NOMA," *IEEE Trans. Commun.*, vol. 70, no. 6, pp. 3912–3929, Jun. 2022.

[20] T. Schenk, *RF Imperfections in High-RateWireless Systems: Impact and Digital Compensation*. Cham, Switzerland: Springer, 2008.

[21] F. Ding, H. Wang, S. Zhang, and M. Dai, "Impact of residual hardware impairments on non-orthogonal multiple access based amplify-and-forward relaying networks," *IEEE Access*, vol. 6, pp. 15117–15131, 2018.

[22] N.-L. Nguyen, S.-P. Le, A.-T. Le, N. D. Nguyen, D.-T. Do, and M. Voznak, "UAV based satellite-terrestrial systems with hardware impairment and imperfect SIC: Performance analysis of user pairs," *IEEE Access*, vol. 9, pp. 117925–117937, 2021.

[23] E. Bjornson, M. Matthaiou, and M. Debbah, "A new look at dual-hop relaying: Performance limits with hardware impairments," *IEEE Trans. Commun.*, vol. 61, no. 11, pp. 4512–4525, Nov. 2013.

[24] M. Li, X. Yu, A. He, and T. Teng, "On the secrecy performance of UAV-assisted wireless communication system with hardware impairments and protected zone," in *Proc. IEEE Int. Conf. Commun. Workshops (ICC Workshops)*, May 2022, pp. 993–998.
[25] K. Guo and K. An, "On the performance of RIS-assisted integrated satellite-UAV-terrestrial networks with hardware impairments and interference," *IEEE Wireless Commun. Lett.*, vol. 11, no. 1, pp. 131–135, Jan. 2022.
[26] Z. Xiong, Y. Zhang, W. Y. B. Lim, J. Kang, D. Niyato, C. Leung, and C. Miao, "UAV-assisted wireless energy and data transfer with deep reinforcement learning," *IEEE Trans. Cognit. Commun. Netw.*, vol. 7, no. 1, pp. 85–99, Mar. 2021.
[27] K. Li, W. Ni, E. Tovar, and M. Guizani, "Joint flight cruise control and data collection in UAV-aided Internet of Things: An onboard deep reinforcement learning approach," *IEEE Internet Things J.*, vol. 8, no. 12, pp. 9787–9799, Jun. 2021.
[28] K. Li, W. Ni, E. Tovar, and A. Jamalipour, "Deep Q-learning based resource management in UAV-assisted wireless powered IoT networks," in *Proc. IEEE Int. Conf. Commun. (ICC)*, Jun. 2020, pp. 1–6.
[29] T. N. Do, G. Kaddoum, T. L. Nguyen, D. B. da Costa, and Z. J. Haas, "Aerial reconfigurable intelligent surface-aided wireless communication systems," in *Proc. IEEE 32nd Annu. Int. Symp. Pers., Indoor Mobile Radio Commun. (PIMRC)*, Sep. 2021, pp. 525–530.
[30] Z. Ding and H. Vincent Poor, "A simple design of IRS-NOMA transmission," *IEEE Commun. Lett.*, vol. 24, no. 5, pp. 1119–1123, May 2020.
[31] T.-T.-T. Dao, S. Q. Nguyen, H. Nhung-Nguyen, P. X. Nguyen, and Y.-H. Kim, "Performance evaluation of downlink multiple users NOMA-enable UAV-aided communication systems over Nakagami-*m* fading environments," *IEEE Access*, vol. 9, pp. 151641–151653, 2021.
[32] Q. Wang, X. Li, S. Bhatia, Y. Liu, L. T. Alex, S. A. Khowaja, and V. G. Menon, "UAV-enabled non-orthogonal multiple access networks for ground-air-ground communications," *IEEE Trans. Green Commun. Netw.*, vol. 6, no. 3, pp. 1340–1354, Sep. 2022.
[33] R. Bajpai, H. Ramesh, N. Gupta, and V. A. Bohara, "Outage analysis of multicarrier full-duplex cooperative UAV-to-UAV communications system," *IEEE Wireless Commun. Lett.*, vol. 12, no. 8, pp. 1309–1313, Aug. 2023.
[34] T. Z. H. Ernest, A. S. Madhukumar, R. P. Sirigina, and A. K. Krishna, "NOMA-aided UAV communications over correlated Rician shadowed fading channels," *IEEE Trans. Signal Process.*, vol. 68, pp. 3103–3116, 2020.
[35] C. Guo, C. Guo, S. Zhang, and Z. Ding, "UAV-enabled NOMA networks analysis with selective incremental relaying and imperfect CSI," *IEEE Trans. Veh. Technol.*, vol. 69, no. 12, pp. 16276–16281, Dec. 2020.
[36] T. Hou, Y. Liu, Z. Song, X. Sun, and Y. Chen, "Multiple antenna aided NOMA in UAV networks: A stochastic geometry approach," *IEEE Trans. Commun.*, vol. 67, no. 2, pp. 1031–1044, Feb. 2019.
[37] M. Matthaiou, A. Papadogiannis, E. Bjornson, and M. Debbah, "Two-way relaying under the presence of relay transceiver hardware impairments," *IEEE Commun. Lett.*, vol. 17, no. 6, pp. 1136–1139, Jun. 2013.
[38] H. V. Nguyen, V.-D. Nguyen, O. A. Dobre, D. N. Nguyen, E. Dutkiewicz, and O.-S. Shin, "Joint power control and user association for NOMA-based full-duplex systems," *IEEE Trans. Commun.*, vol. 67, no. 11, pp. 8037–8055, Nov. 2019.
[39] P. K. Sharma and D. I. Kim, "UAV-enabled downlink wireless system with non-orthogonal multiple access," in *Proc. IEEE Globecom Workshops (GC Wkshps)*, Dec. 2017, pp. 1–6.
[40] T. M. Hoang, B. C. Nguyen, L. T. Dung, and T. Kim, "Outage performance of multi-antenna mobile UAV-assisted NOMA relay systems over Nakagami-*m* fading channels," *IEEE Access*, vol. 8, pp. 215033–215043, 2020.
[41] S. Q. Nguyen, A.-T. Le, C.-B. Le, P. T. Tin, and Y.-H. Kim, "Exploiting user clustering and fixed power allocation for multi-antenna UAV-assisted IoT systems," *Sensors*, vol. 23, no. 12, p. 5537, Jun. 2023.
[42] D.-T. Do and A.-T. Le, "NOMA based cognitive relaying: Transceiver hardware impairments, relay selection policies and outage performance comparison," *Comput. Commun.*, vol. 146, pp. 144–154, Oct. 2019.
[43] F. Ono, H. Ochiai, and R. Miura, "A wireless relay network based on unmanned aircraft system with rate optimization," *IEEE Trans. Wireless Commun.*, vol. 15, no. 11, pp. 7699–7708, Nov. 2016.
[44] M. K. Simon and M.-S. Alouini, *Digital Communication Over Fading Channels*, 2nd ed. New York, NY, USA: Wiley, 2005.
[45] F. Tan, H. Chen, and F. Zhao, "Performance analysis of energy harvesting multi-antenna relaying system over mixed Nakagami-*m*/Rician fading channels," *Phys. Commun.*, vol. 34, pp. 157–164, Jun. 2019.
[46] P. K. Mittal and K. C. Gupta, "An integral involving generalized function of two variables," *Proc. Indian Acad. Sci. Sect. A*, vol. 75, no. 3, pp. 117–123, Mar. 1972.
[47] D.-T. Do, A.-T. Le, and B. M. Lee, "NOMA in cooperative underlay cognitive radio networks under imperfect SIC," *IEEE Access*, vol. 8, pp. 86180–86195, 2020.
[48] H. Lu, Y. Zeng, S. Jin, and R. Zhang, "Aerial intelligent reflecting surface: Joint placement and passive beamforming design with 3D beam flattening," *IEEE Trans. Wireless Commun.*, vol. 20, no. 7, pp. 4128–4143, Jul. 2021.
[49] I. S. Gradshteyn and I. M. Ryzhik, *Tables of Integrals, Series and Products*, 6th ed. New York, NY, USA: Academic Press, 2000.
[50] H. Lei, I. S. Ansari, G. Pan, B. Alomair, and M.-S. Alouini, "Secrecy capacity analysis over $\alpha - \mu$ fading channels," *IEEE Commun. Lett.*, vol. 21, no. 6, pp. 1445–1448, Jun. 2017.
[51] K. P. Peppas, "A new formula for the average bit error probability of dual-hop amplify-and-forward relaying systems over generalized shadowed fading channels," *IEEE Wireless Commun. Lett.*, vol. 1, no. 2, pp. 85–88, Apr. 2012.
[52] M. Abramowitz and I. A. Stegun, *Handbook of Mathematical Functions with Formulas, Graphs, and Mathematical Tables*. New York, NY, USA: Dover, 1972.
[53] A. P. Prudnikov, Y. A. Brychkov, and O. I. Marichev, *Integrals and Series, Volume 3: More Special Functions*. New York, NY, USA: Gordon and Breach, 1986.

BUI VU MINH was born in Dong Nai, Vietnam, in March 1991. He received the degree in electrical and electronic engineering from Nguyen Tat Thanh University, Ho Chi Minh City, Vietnam, in 2014, and the master's degree in engineering electrical from the Ho Chi Minh City University of Technology and Education, in 2019. In 2014, he joined the Faculty of Electrical and Electronics, Nguyen Tat Thanh University, as a Laboratory-Practice Management, where he was a Lecturer, until 2017. His current research interests include artificial neuron networks, fuzzy logic, and wireless networks.

ANH-TU LE (Member, IEEE) was born in Lam Dong, Vietnam, in 1997. He received the B.S. degree from the Industrial University of Ho Chi Minh City, Vietnam, in 2019, and the M.S. degree from Ton Duc Thang University, Vietnam, in 2022. He has authored and coauthored more than 25 ISI-indexed journals. His current research interests include wireless channel modeling, NOMA, cognitive radio, MIMO, and machine learning.

CHI-BAO LE was born in Binh Thuan, Vietnam. He is currently pursuing the master's degree in wireless communications. His current research interests include signal processing in wireless communications networks, nonorthogonal multiple access, and physical-layer security.

SANG QUANG NGUYEN received the B.E. degree from the Ho Chi Minh City University of Transport, Vietnam, in 2010, the M.E. degree from the Ho Chi Minh City University of Technology, Vietnam, in 2013, and the Ph.D. degree in electrical engineering from the University of Ulsan, South Korea, in 2017. From January 2017 to June 2017, he was a Postdoctoral Research Fellow with Queen's University Belfast. From July 2017 to April 2021, he was a Lecturer with Duy Tan University, Vietnam. Since May 2021, he has been a Lecturer with the Ho Chi Minh City University of Transport. His current research interests include cooperative communication, cognitive radio, physical layer security, energy harvesting, non-orthogonal multiple access, and unreliable backhaul connections.

VAN-DUC PHAN was born in Long An, Vietnam, in 1975. He received the M.S. degree from the Department of Electric, Electrical and Telecommunication Engineering, Ho Chi Minh City University of Transport, Ho Chi Minh, Vietnam, and the Ph.D. degree from the Department of Mechanical and Automation Engineering, Da-Yeh University, Taiwan, in 2016. His current research interests include sliding mode control, non-linear systems or active magnetic bearing, flywheel store energy systems, power system optimization, optimization algorithms, renewable energies, energy harvesting (EH) enabled cooperative networks, improving the optical properties, lighting performance of white LEDs, energy efficiency LED driver integrated circuits, novel radio access technologies, and physical security in communication networks.

TAN N. NGUYEN (Member, IEEE) was born in Nha Trang, Vietnam, in 1986. He received the B.S. degree in electronics from the Ho Chi Minh University of Natural Sciences, in 2008, the M.S. degree in telecommunications engineering from Vietnam National University, in 2012, and the Ph.D. degree in communications technologies from the Faculty of Electrical Engineering and Computer Science, VSB—Technical University of Ostrava, Czech Republic, in 2019. He joined the Faculty of Electrical and Electronics Engineering, Ton Duc Thang University, Vietnam, in 2013, and since then he has been lecturing. His current research interests include cooperative communications, cognitive radio, signal processing, satellite communication, UAV, and physical layer security. He is the Editor-in-Chief of *Advances in Electrical and Electronic Engineering* (AEEE) journal, in 2023.

MIROSLAV VOZNAK (Senior Member, IEEE) received the Ph.D. degree in telecommunications from the Faculty of Electrical Engineering and Computer Science, VSB—Technical University of Ostrava, and the Habilitation degree, in 2009. He was appointed as a full professor of electronics and communications technologies, in 2017. He is a Principal Investigator in the research project QUANTUM5 funded by NATO, which focuses on the application of quantum cryptography in 5G campus networks. He has participated in six projects funded by the EU in programs managed directly by the European Commission. He has authored and coauthored more than 100 articles in SCI/SCIE journals. His current research interests include ICT, especially on quality of service and experience, network security, wireless networks, and big data analytics. According to the Stanford University study released, in 2020, he is one of the World's Top 2% of Scientists in networking and telecommunications, and information and communications technologies. He has served as the General Chair for the 11th IFIP Wireless and Mobile Networking Conference, in 2018, and the 24th IEEE/ACM International Symposium on Distributed Simulation and Real-Time Applications, in 2020.